# A Spotter's Guide to Dispersion in Surface-Confined Voltammetry Experiments

Henry O. Lloyd-Laney,[†] Martin J. Robinson,[†] Alan M. Bond,[‡] Alison Parkin,[*,¶] and David J. Gavaghan[*,†]

[†]*Department of Computer Science, University of Oxford, Wolfson Building, Parks Road, Oxford, OX1 3QD United Kingdom*

[‡]*School of Chemistry and the ARC Centre of Excellence for Electromaterials Science, Monash University, Clayton, Vic., 3800 Australia*

[¶]*Department of Chemistry, University of York, Heslington, York, YO10 5DD, United Kingdom*

E-mail: alison.parkin@york.ac.uk; david.gavaghan@dtc.ox.ac.uk

## Abstract

Dispersion has long been acknowledged as a complicating factor in the analysis of both solution and surface-confined voltammetry experiments. In this tutorial paper, we show how varying levels of dispersion can affect the appearance of the experimental current. We focus on three voltammetric techniques, ramped Fourier Transform AC Voltammetry, Purely Sinusoidal Voltammetry and Direct Current Voltammetry. As modelling dispersion significantly increases the computational burden of simulating voltammetry experiments, making well-informed choices about when to include this effect is essential. To facilitate this, we discuss the intuition for when to include dispersion when fitting experimental voltammetry data, again with reference to the three techniques described above.

1

# Introduction

Simulations of voltammetry experiments conducted on surface-confined ("film") redox species are generated by solving an ordinary differential equation (ODE)[1] that describes the current response of a redox system to a time-varying potential input with given chemical and experimental parameters; we refer to this as solving the forward problem. In parameter inference for experimental data, the goal is to determine the simulation parameters which best describe this data; we refer to this process as solving the "inverse problem".[2] There is a small galaxy of work on solving the inverse problem in electrochemistry, using a battery of computational and mathematical techniques. The approach of fitting computational predictions to experimental data is reviewed in work by Gavaghan[2] and Bieniasz.[3] Other approaches include using quantitative relationships between features of the experimental current and reaction parameters, for example in work by Zouraris,[4] Bell[5] and Laviron.[6]

When solving the inverse problem, in our previous work we have used both optimisation and Markov Chain Monte Carlo (MCMC) methods. In optimisation, we attempt to find the vector of parameters that minimises the distance between the resultant simulation and experimental data. When using MCMC methods we repeatedly sample from regions of parameter space, and by assessing the history of the sampling we obtain an estimate for the likely distribution of parameters. Consequently, depending on the choice of algorithm, the inferred result can be a single vector of $n_p$ parameters,[7] or a set of $M$ samples from an $n_p$-dimensional posterior distribution. Our reasoning for using MCMC sampling over optimisation methods is laid out in the review cited above.[2]

In order to obtain good agreement between experimental data and simulation, we have found that it is necessary to assume that there will be dispersion of the behaviour of the reaction occurring on the surface of the electrode. Dispersion corresponds to an underlying distribution of certain parameter values; this is distinct from an inferred distribution as re-

covered by MCMC methods, which represent uncertainty about point values of parameters. Dispersion has been acknowledged as a complicating factor in the analysis of surface-confined voltammetry experiments since at least the 1990s,[8–10] and has been demonstrated and quantified for a range of systems with multiple different methods. These studies have focussed on dispersion in two key parameters, the rate constant for electron transfer ($k_0$) and the reversible potential ($E^0$), which is a measure of the thermodynamic driving force required for an electrochemical reaction.[11–13] We refer to these two forms as kinetic and thermodynamic dispersion, respectively. It should be noted that, for solution phase voltammetry, which we do not analyse here, it is not possible to have a distribution in the $E^0$ parameter.[14] For a two electron catalytic oxidation reaction, Léger et al.[15] showed that the presence of dispersion in $k_0$ could be detected by a change in the relationship between overpotential and observed current, in a study of the $H_2$-oxidising ability of a [NiFe]-hydrogenase, which has been replicated in additional studies of the protein.[16] Patil et al.[13] detected dispersion in the reversible, non-catalytic single electron-transfer chemistry of the protein azurin through the addition of a Forster resonance donor that fluoresces when reduced, allowing for quantification of the distribution of reversible potentials (as defined by the Nernst equation).[13] This technique was extended by recording fluorescence movies, such that the reversible potentials and rate constants of distinct parts of the electrode could be determined.[12] When these values were binned and plotted as a histogram, the resulting appearance was used by Morris[11] to suggest the true distribution of kinetic and thermodynamic parameters that generated the observations[12] were lognormal and normal respectively.[1]

The assumption that the redox-reactivity of all the subject molecules in the experiment can be described by the same reaction parameter values (i.e. no dispersion) is just one of a

---

[1]A lognormal distribution of kinetic values can also be observed when attempting to solve the inverse problem and a logarithmic transform has been applied when non-dimensionalising the kinetic parameter. Normally distributed uncertainty about the dimensionless kinetic value would result in lognormally-distributed uncertainty about the dimensional kinetic value. It should be noted that this effect is distinct from an underlying spread of kinetic values, and could be observed even if the true distribution was a delta function.

series of assumptions introduced to simplify the simulation of surface-confined voltammetric experiments. Additional assumptions include the choice of isotherm[17] and the theory used to describe electron transfer.[18] In terms of isotherm, the Langmuir isotherm is the simplest, assuming non-interaction between individual chemical moieties, while other isotherms, such as the Freundlich, Temkin and Frumkin isotherms include terms for the interaction of these species, along with different descriptions for their adsorption behaviours. The rate of electron transfer can be described by Butler-Volmer theory,[19] Marcus theory[20] or other quantum approaches.[21] While we only address the presence of dispersion in this piece of work, it should be noted that all three assumptions have areas of conceptual overlap; for example, the Temkin isotherm assumes a distribution of adsorption states, along with molecule self-interaction, which could lead to dispersion-like behaviours. Consequently, the experimental artefacts we ascribe to dispersion are likely the result of a highly complex surface chemistry. We have focussed on dispersion in this case as it has recieved more extensive attention in the theoretical literature,[11] with most models of voltammetry experiments assuming a Langmuir isotherm and Butler-Volmer kinetics, although there are exceptions.[21]

When analysing surface-confined voltammetry data, obtaining the solution to the forward problem when dispersion is incorporated is significantly more computationally taxing. In addition, modelling the dispersion effects adds more degrees of freedom to the inverse problem due to the need to parameterise a probability distribution for each dispersed parameter, resulting in a greater frequency of spurious results (e.g. due to becoming trapped in local minima). Consequently, determining which form of dispersion is present (if at all), and the likely order of magnitude for the required parameters, is an essential step in the process of solving the inverse problem in reasonable time. The purpose of this paper is to communicate the effect that dispersion of key parameters has on the current response in a range of surface-confined voltammetry experiments, and to act as a reference for when the nature of the dispersion is ambiguous, such that appropriate choices about where to include dispersion

can be made.

In this work, we focus on the effect of including dispersion on three experimental techniques; ramped Fourier transform alternating current voltammetry (FTACV), purely sinusoidal voltammetry (PSV) and direct current voltammetry (DCV). Assuming the chemical reaction parameters for an electrode film are independent of input potential, the current output from different voltammetric protocols should be well described by one parameter vector, allowing for variation introduced by temporal separation and artefacts peculiar to the specific protocol. Consequently, if an inferred parameter vector describes one experiment well but not the others, this suggests that the inferred parameters represent a local rather than the global minimum in parameter space. We have specifically chosen these protocols as they have contrasting areas of strength and weakness. The potential inputs of ramped FTACV and PSV both include large-amplitude sinusoids, which means that the Faradaic current response to these inputs is non-linear, resulting in harmonics of the frequency of the input sinusoid. These harmonics can be individually selected by use of the Fourier Transform, and the higher harmonics are largely free of the "background" non-Faradaic current from double-layer capacitance.[19,22] The harmonics of ramped FTACV in particular are information rich, and highly sensitive to dispersion. PSV by contrast, is a simpler technique that contains less information and is less sensitive to dispersion, but is much faster to simulate than the ramped FTACV experiment, by at least an order of magnitude.[23] DCV takes approximately the same time to simulate as PSV, and is included because of its widespread use amongst the electrochemistry community. This paper builds on the basic theoretical work described in,[11] extending the analysis to PSV and DCV, and including sensitivity information about the various dispersion parameters.

# Mathematical model

Throughout this paper we will consider the simplest possible experimental system, that of a surface-confined 1-electron redox reaction, with the surface processes assumed to be controlled by Butler Volmer kinetics and a Langmuir isotherm. In our previous work we have described how this system can be modelled by a system of ordinary differential equations, with the three different experimental protocols of FTACV, PSV and DCV being modelled through changes in the terms describing the applied potential. The equations used throughout this paper can be found in.[1,19] To model the dispersion of a subset of $n_p$ of the parameters, we follow the procedure described below.

We assume that any parameter which is affected by dispersion no longer has a single fixed value but instead is drawn from a probability distribution which captures the degree of the dispersion. If we have $n_p$ dispersed parameters in the model, then we assume that in any particular experiment, those $n_p$ parameters are drawn from a joint probability $\phi(p_1, p_2, ..., p_n)$. The total current recorded given the distribution is the expectation $E[I(t, (p_1, ..., p_n))]$, which we refer to as $I_{disp}$[11]

$$I_{disp} = \int_{A_n} ... \int_{A_1} I(t, (p_1, ..., p_n))\phi(p_1, p_2, ..., p_n)dp_1...dp_n, \tag{1}$$

where $I(t, (p_1, ..., p_n))$ is the simulated current $I$ as a function of time and the $n_p$ dispersed parameters $p_1, p_2, ..., p_n$. The range of the $i^{th}$ integral is represented as $A_i$. This integral cannot be calculated analytically, and so we approximate it with numerical quadrature.

## Numerical quadrature

We describe two numerical quadrature approaches here for a single parameter (i.e. the calculation of $E[I(t, p)]$), but they can be easily combined for multiple integrals, as in the expression in equation 1. The same principle can be applied to both methods; the function to

be integrated is evaluated at points over the range of the integral, and these evaluations are weighted appropriately and summed. This is represented in figure 1, where, the distribution has been partitioned in equally-spaced "bins". The sum of the area of all bins (such as the one filled in blue) is an approximation to the value of the integral.
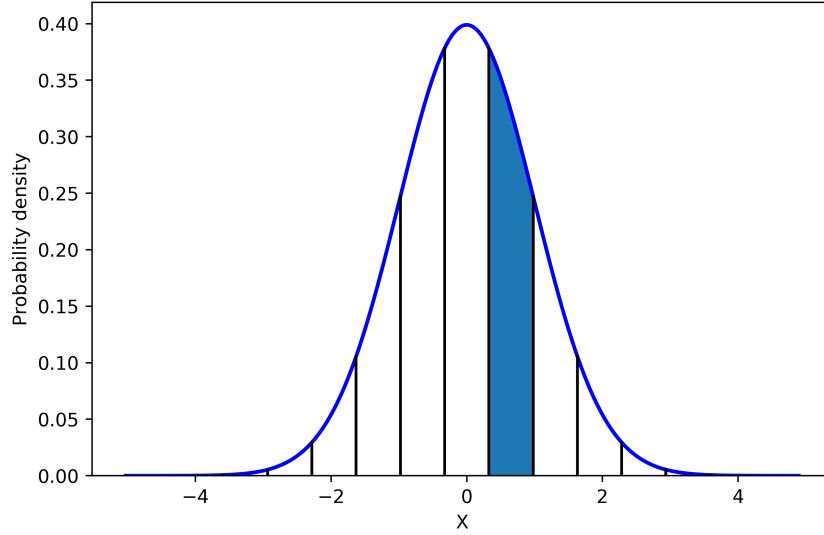


Figure 1: A representation of numerical integration of a Gaussian distribution

## Midpoint rule

The midpoint rule for the integral of a function $f(x)$ is

$$\int_b^a f(x)dx \approx (b-a)f\left(\frac{b+a}{2}\right). \tag{2}$$

In order to approximate the value of the expectation $E[I(t,p)]$ using this rule, for a chosen number of bins $N_b$, we use the expression

$$E[I(t,p)] \approx \sum_{i=1}^{N_b} w_i I\left(\left(\frac{b_i + b_{i-1}}{2}\right), t\right), \tag{3}$$

7

where the set of parameter values is $b_0, ..., b_{N_b}$ and the weight $w_i$ is calculated using the midpoint rule such that

$$w_i = (b_i - b_{i-1})f\left(\frac{b_i + b_{i-1}}{2}\right),\tag{4}$$

or alternatively

$$w_i = F(p_i) - F(p_{i-1}),\tag{5}$$

where $f$ and $F$ are the probability density and cumulative density functions for the parameter distribution $\phi(p)$ respectively. As the support for many distributions is infinite, for numerical purposes we define the parameter range to integrate over (i.e. $p_0, ..., p_n$) using the inverse cumulative density function $F^{-1}$, such that $p_0 = F^{-1}(x)$ and $p_n = F^{-1}(1-x)$. The area of an integral over $f$ defined by this range of values will be $\sim 1 - 2x$, and so we choose a value for $x$ that is small enough such that $\sum_{i=1}^{n} w_i \approx 1$.

## Gauss-Hermite quadrature

When approximating $E[I(t,p)]$ when the distribution $\phi(p)$ is Gaussian, we can use Gauss-Hermite quadrature, which achieves better accuracy than the midpoint rule, and is valid for integrals over the range $[-\infty, \infty]$. By choosing the positions at which to evaluate the function (the nodes), and weighting it appropriately, Gauss-Hermite quadrature can exactly calculate the integrals of polynomial functions of degree 2n-1 in the form $e^{-x^2}f(x)$ using $N_b$ nodes, such that

$$\int_{-\infty}^{\infty} e^{-x^2} f(x)dx = \sum_{i=0}^{N_b} w_i f(x_i).\tag{6}$$

To make this appropriate for the calculation of the expectation of a Gaussian distribution, we write the calculation for $E[I(t,p)]$ in the form

$$E[I(t,p)] = \int_{-\infty}^{\infty} \frac{1}{\sigma\sqrt{2\pi}} \exp\left(\frac{-(p-\mu)^2}{2\sigma^2}\right) I(p,t)dp,\tag{7}$$

where $\mu$ and $\sigma$ are mean and standard deviation of the normal distribution. If we transform $p$ such that $p = \sigma\sqrt{2x} + \mu$, then

$$E[I(t,p)] = \int_{-\infty}^{\infty} \frac{1}{\sqrt{\pi}} \exp\left(-x^2\right) I(\sigma\sqrt{2x} + \mu, t)dx, \tag{8}$$

consequently, for a Hermite polynomial of degree $N_b$

$$E[I(t,p)] \approx \sum_{i=1}^{N_b} \frac{1}{\sqrt{\pi}} w_i I(\sigma\sqrt{2x_i} + \mu, t)dx, \tag{9}$$

where $x_i$ and $w_i$ are the zeros and appropriate weights of the Hermite polynomial of degree $N_b$ respectively, and the weights are calculated using the Golub-Welsch algorithm.

## Results and Discussion

In order to show the effect each dispersion parameter has, we perform parameter scans where all parameters are held constant except the one of interest. Although the effect observed from this process may not be exclusive to the parameter in question (as other parameters have the same effect), and there may be parameter regimes where the observed effect is less apparent, this process is the easiest way to gain intuition about the effects of the various parameters. Intuition about the approximate order of magnitude for the dispersion parameters allows the experimentalist to constrain parameter space (for either heuristic or automatic inference approaches). The more parameter space is constrained, the easier it is to find the global optimum, as long as the constraint process has not, in fact, excluded this optimum. In figures 2-4, we show the results of holding all parameters constant (as reported in table 1) except the parameter named in the upper left hand corner of each plot, the value of which is indicated. We have chosen this range of parameters as a compromise between clear visual separation between different parameter values, and chemical realism. For this reason, the parameters that contribute to the background current (the capacitance and uncompensated resistance) are

in the lower range of what would be observed in a typical voltammetry experiment, and the surface coverage is in the higher range. The experimental parameters are taken from a PSV experiment, performed on a glassy carbon electrode modified with Cytochrome C oxidase. The reversible potential parameters are from the parameterisation of this same experiment. The kinetic parameters were chosen as a compromise between providing the "ideal" ramped harmonic appearance, and sensitivity to these parameters (all kinetic distributions where the majority of the range is approaching or exceeding the reversible limit will look identical). In the SI, we have included equivalent plots for the irreversible to quasi-reversible regime, (i.e. $k_0 = 1$) for all three experiments, see figures S1-S3. With regards to the choice of distribution, for the reversible potential $E^0$, we use a skewed Gaussian distribution (where a skew of zero is a regular Gaussian), and for the rate constant $k_0$ we use a lognormal distribution. The choice of a Gaussian and lognormal distributions are informed by previous work.[11,12] The skew parameter was included as observations of ramped FTACV data in our previous work implied the presence of an asymmetric distribution of $E^0$ values,[23] which for normally distributed values indicates the presence of skew. Although other parameters are suspected of being dispersed, such as the symmetry factor $\alpha$[23] and the uncompensated resistance, we neglect them here due to space constraints. For each subgroup of plots, the input parameter distribution is shown on the top, and the resultant current-potential output is shown below.

For the the ramped experiment, we show harmonics 3, 5 and 7 plotted against time instead of a current-potential plot, as the harmonics are more sensitive to dispersive effects, and are easily interpretable. In terms of the thermodynamic distribution parameters, the value of the mean of the distribution $E^0\mu$ affects the position of the harmonic relative to the potential, and the magnitude of the harmonic increases the closer the value of the $E^0\mu$ is to the reverse potential. The standard deviation of the distribution $E^0\sigma$ affects the both the width and magnitude of the harmonic, with higher harmonics being affected more strongly. The skewness of the distribution $E^0\kappa$ has a slightly more complex effect — the skewed dis-

Table 1: Simulation parameters used to generate plots in the main body of this paper. For some experimental parameters, the simulation value is different for each technique, and is written in the following order: ramped FTACV/PSV/DCV, with a * indicating that the parameter is not used in the simulation

| Parameter | Symbol | Value |
|---|---|---|
| Start potential | $E_{start}$ (V) | -0.5 |
| Reverse potential | $E_{reverse}$ (V) | 0.1 |
| Reversible potential | $E^0$ (V) | -0.25 |
| Rate constant | $k_0(s^{-1})$ | 100 |
| Uncompensated resistance | $R_u$ ($\Omega$) | 0.0 |
| Double-layer capacitance | $C_{dl}$ (F) | 1.0E-5 |
| Surface coverage | $\Gamma$ (mol cm$^{-2}$) | 1.0E-10 |
| Symmetry factor | $\alpha$ | 0.5 |
| Scan rate | v ($Vs^{-1}$) | 0.022/*/1 |
| Potential frequency | $\omega$ (Hz) | 8.881/8.94/* |
| Phase | Phase (rads) | $0.0/\frac{3\pi}{2}/*$ |
| Potential amplitude | $\Delta E$ (V) | 0.15/0.3/* |
| Sampling rate | $(s^{-1})$ | 400.0 |
| Electrode Area | Area ($cm^2$) | 0.07 |
| Reversible potential mean | $E^0\mu$ (V) | -0.25 |
| Reversible potential standard deviation | $E^0\sigma$ (V) | 0.05 |
| Reversible potential skew | $E^0\kappa$ | 0.0 |
| Rate constant shape | $\log(k^0(s^{-1}))\sigma$ | 0.5 |
| Rate constant scale | $\log(k^0(s^{-1}))\mu$ | 100 |

tributions are less broad than the unskewed distribution (i.e. $E^0\kappa = 0$), which accounts for why the magnitude of each skewed harmonic is larger than for the unskewed harmonic. In addition, the presence of skew means that the position of the harmonic within the timeseries is a function of the order of the harmonic.

The effect of the parameters for the lognormal $k_0$ distribution on the simulation output are less immediately obvious. Increasing the scale parameter (which is the mean of the natural logarithm of $k_0$, i.e. $\log(k^0)\mu$) largely effects the resolution of the individual harmonics, with the higher harmonics being more sensitive to this effect; this is especially apparent in the $7^{th}$ harmonic, where the peaks of the green plot are less well-resolved than the blue and

orange plots, which have a higher $\log(k^0)\mu$ value. As expected, this is similar to the effect of altering the value of $k_0$ as a point value. The $\log(k^0)\sigma$ parameter, which also affects the width of distribution has the effect of reducing the magnitude of the harmonics, where the higher harmonics are also more strongly affected. This is distinct from the $E^0\sigma$ parameter, which reduces *and* broadens the harmonics.
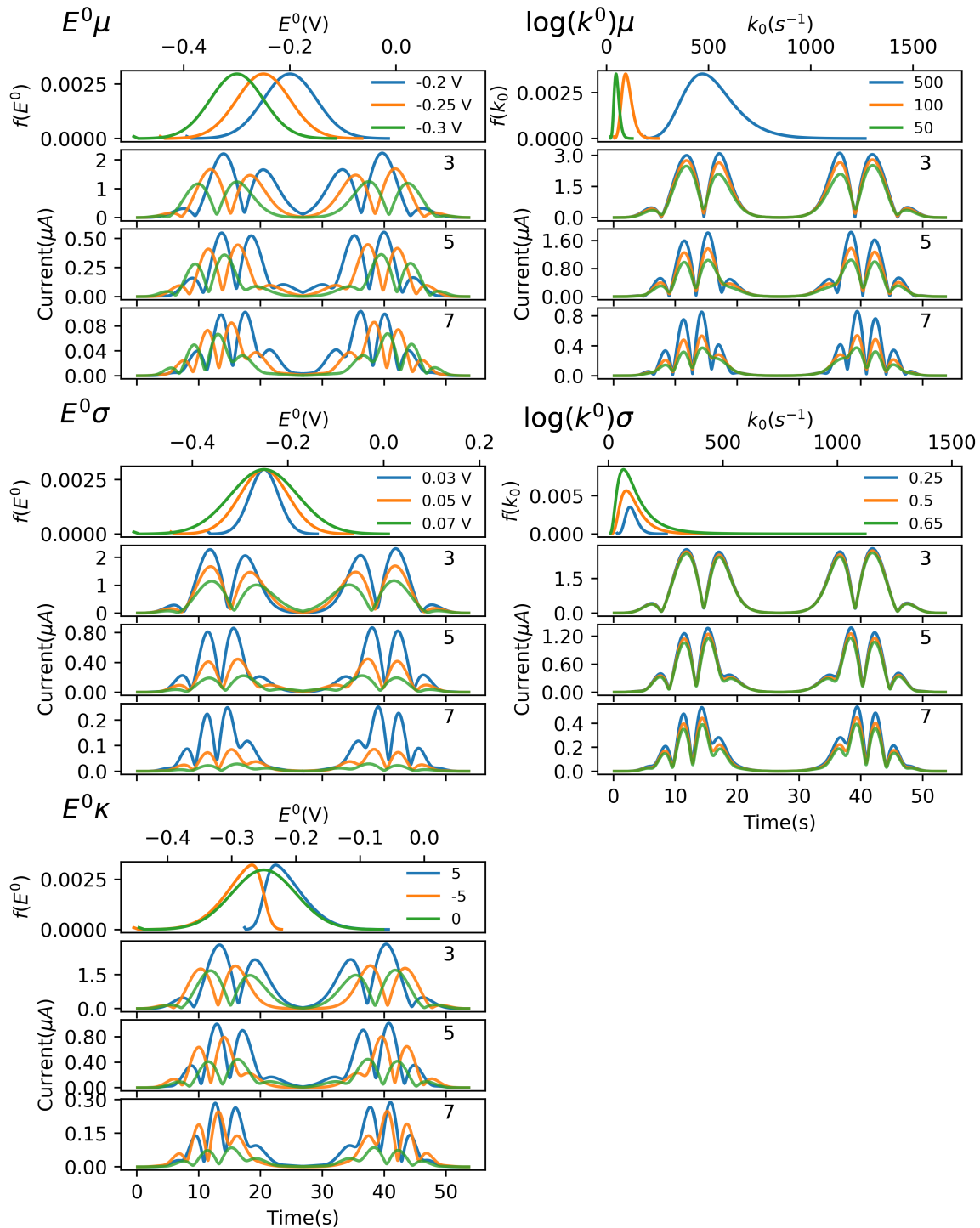
Figure 2: Plots of simulated ramped FTACV harmonics vs time , with dispersion parameters for $E^0$ — mean, standard deviation and skew $(E^0\mu, E^0\sigma, E^0\kappa)$ and $k_0$ — shape and scale $(\log(k_0)\mu, \log(k_0)\sigma)$ where the parameter being varied is in the top left hand corner. The resulting distribution, where $f$(parameter) is the probability density, is shown at the top of the plot, and the $3^{rd}$, $5^{th}$ and $7^{th}$ harmonics shown. The colour of the harmonic corresponds to the colour of the distribution. Simulation parameters are found in table 1. For all cases, the kinetics of the reaction are in the reversible regime.

For the PSV case (figure 3), we assess the effect of each parameter on the current-potential plots, instead of the harmonics. This is because the harmonics of the PSV timeseries are not as amenable to immediate visual interpretation as the harmonics of the ramped experiment. The effects of the various thermodynamic and kinetic dispersion parameters are similar for PSV and DCV (figure 4), which is not unexpected. The reason for this similarity is that the PSV potential input is highly similar to multiple cycles of the DCV potential input, except without a discontinuity at the switching potential, and the fact that the PSV input elicits a non-linear current response. With this similarity in mind, we note that the effect of each parameter controlling the shape of the $E^0$ distribution on both the PSV and DCV current-potential outputs is as described for the ramped FTACV harmonics, namely $E^0\mu$ alters the position of the reductive and oxidative peaks, $E^0\sigma$ broadens and reduces the magnitude of these peaks, and $E^0\kappa$ affecting the position and amplitude of the peak. The effect of the $k_0$ distribution parameters however, are different for ramped-FTACV harmonics and PSV/DCV current-potential plots. For the PSV plots, the $\log(k^0)\mu$ parameter also exerts a similar effect to the one described for the ramped harmonics, i.e. similar to the effect of $k_0$ as a point value. The exact nature of this effect depends upon which regime (irreversible, quasi-reversible or reversible) the dimensionless $k_0$ value is in. In more detail, for current-potential PSV plot of a completely reversible system, the oxidative and reductive peaks will be stacked on top of one another. As the kinetics becomes progressively slower, the relative peak position will start to diverge, along with peak broadening and a reduction in maximum amplitude. The parameter $\log(k^0)\sigma$ affects the gradient of the current returning from a Faradaic peak to background current. As the effects of the kinetic parameters are similar for both the DCV and PSV timeseries, for the DCV case (figure 4) we also show trumpet plots — this method, as introduced by Laviron[6] plots the potential value at which the oxidative and reductive peaks are observed, plotted against the logarithm of the scan rate, and is used for inferring the kinetic value in DCV experiments. The $\log(k^0)\sigma$ parameter slightly reduces the gradient of the oxidative and reductive curves. The $\log(k^0)\mu$ parameter alters the scan

rate at which the locations for the oxidative and reductive peaks start to diverge.

The descriptions of all of the effects of these parameters are caveated with the fact that varying other parameters used in the simulation of the current response can have similar effects. Obtaining an understanding of the effects and interactions of the various parameters requires iteratively comparing multiple simulations. As this is not feasible in the static format of a journal article, we have developed an online interactive application for the 1-electron redox case. This can be found here, and allows the user to simulate the three experiments described in this paper, with or without dispersion, and compare multiple different simulations. The app can also be run locally using the source code hosted in the associated Github repository.
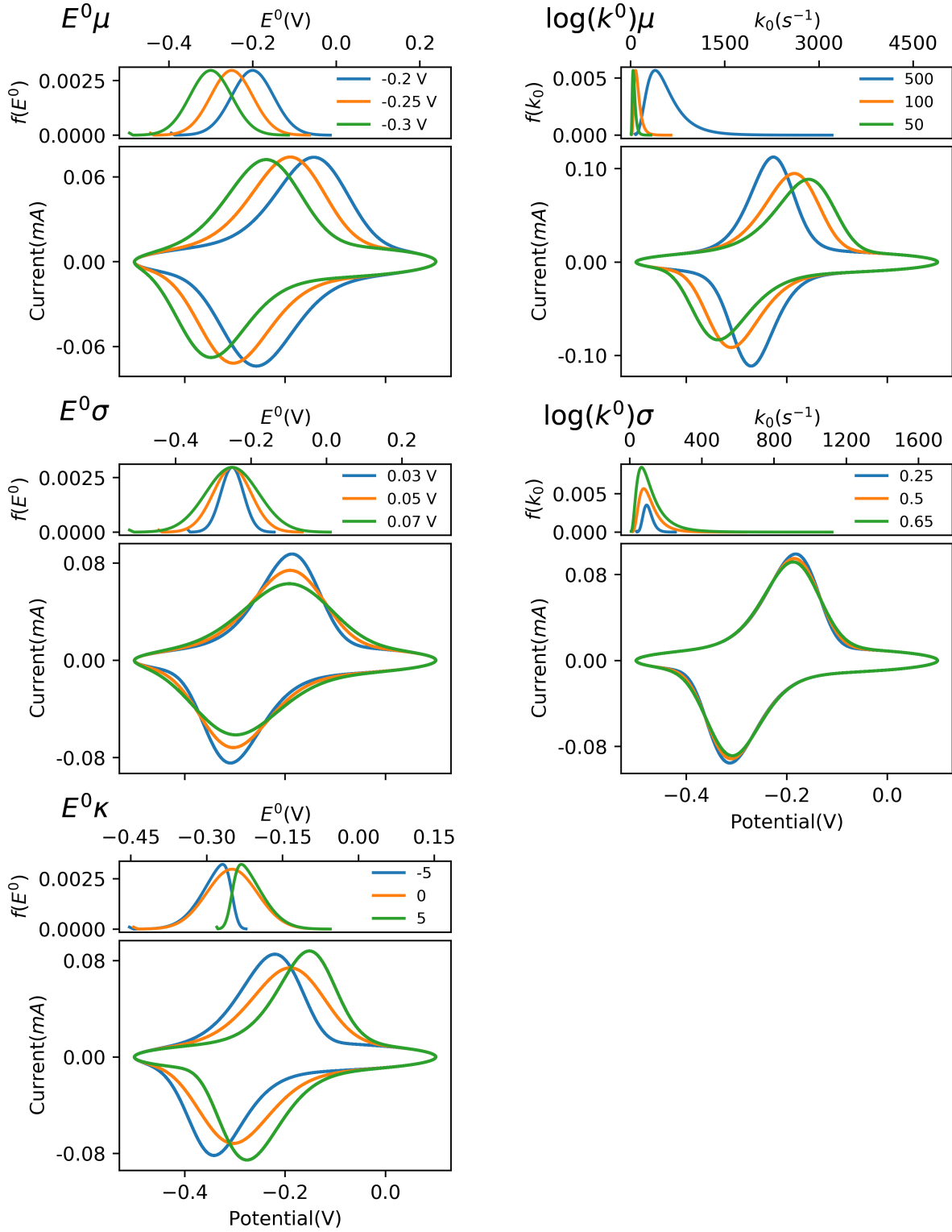
Figure 3: Parameter scans for a PSV current-potential plot, where the parameter distributions under investigation are plotted in the top panel of each plot subgroup. The remaining simulation parameters can be found in table 1
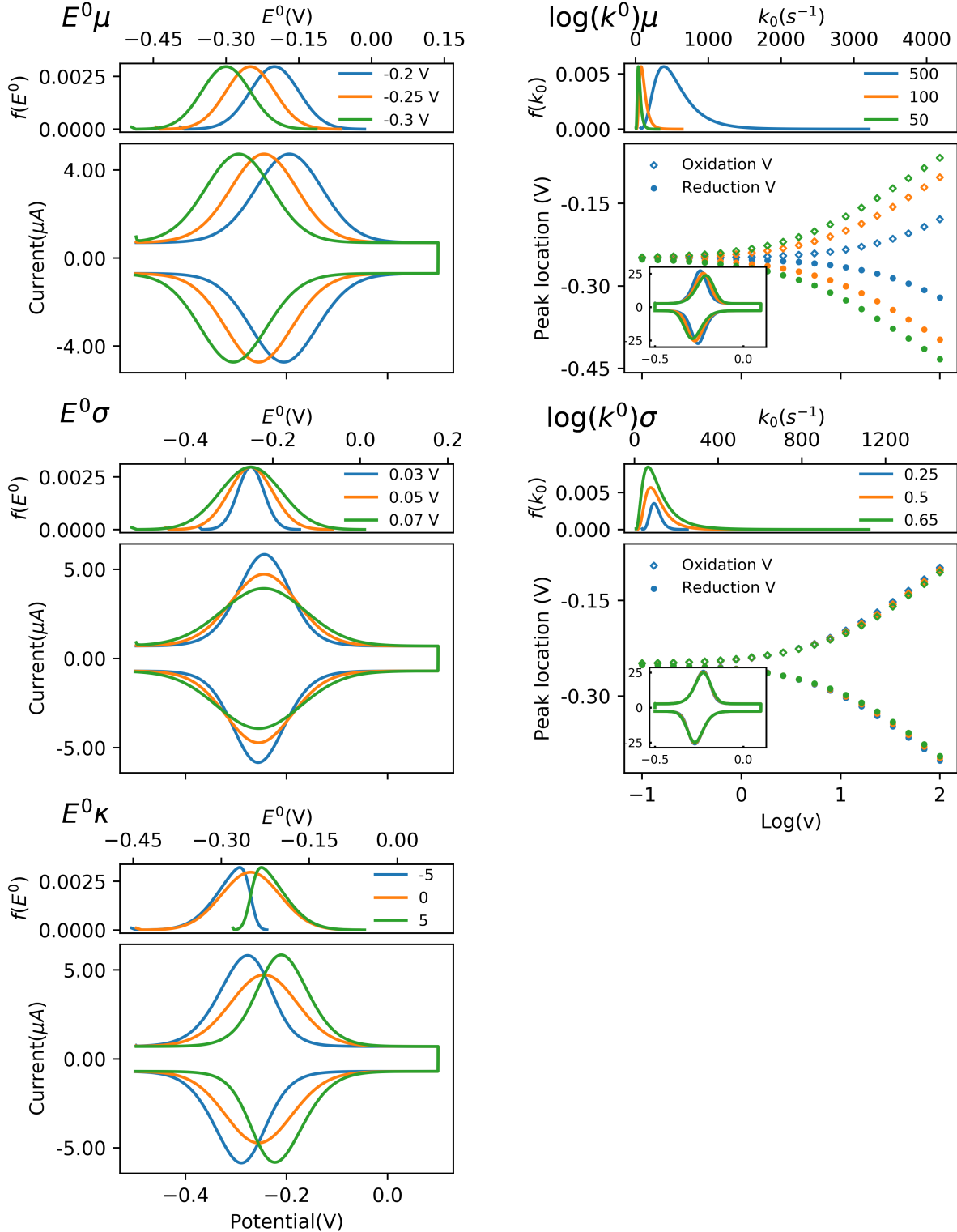
Figure 4: Parameter scans for a DCV current-potential plot (left), and trumpet plots (right) which plot the potential-values of the maximum and minimum current peaks against the logarithm of the scan rate. The inset plot in the right hand column is a current($\mu$A)-potential(V) plot of a DCV simulation using a scan rate from the middle of the range defined in the $x$-axis of the containing plot. The remaining simulation parameters can be found in table 1

## Distinguishing different forms of dispersion

In figure 5, we show the effects of dispersion for three cases, $E^0$, $k_0$ and a combination of the two, as shown in the legend, relative to the non-dispersed case, which is marked as "None". Distinguishing between purely thermodynamic and purely kinetic dispersion is relatively simple, at least in the ramped case, as, while both result in a reduction in the expected magnitude of the harmonic (with the higher harmonics being more sensitive to this effect), only $E^0$ broadens it. The difficulty lies in resolving a combination of $E^0$ and $k_0$ dispersion from pure $E^0$ dispersion, as the latter dominates. This is also complicated by the fact that the reduction in harmonic magnitude is also an effect of other parameters, such as the uncompensated resistance. As before, both the PSV and DCV cases are less sensitive to the presence of dispersion and more challenging to interpret. For DCV, instead of showing current-potential plots for cases involving kinetic dispersion, we have used trumpet plots. Here, there is a slight difference in gradient between the kinetically-dispersed, thermodynamically dispersed and non-dispersed cases. In figure S4, we show that when $k_0$ is highly reversible, the presence of $k_0$ dispersion is identical to the non-dispersed case, and in figure S5 we show that the effect of $k_0$ is greatest relative to the non-dispersed case in the irreversible and quasi-reversible regimes. This is because the timeseries is more sensitive to changes in $k_0$ in these regimes, and consequently a distribution of values has a greater effect. Consequently increasing either the scan rate (for DCV) or the input frequency (for ramped FTACV and PSV) will therefore make the results of the experiment more sensitive to kinetic dispersion. It is possible to quantify this by assessing the distance between the dispersed and non-dispersed cases, and selecting the input frequency that delivers the greatest amount of distance, an example of which we show in figure S6. It should also be noted that a separation between thermodynamic and kinetic dispersion is somewhat arbitrary. Marcus theory predicts that the thermodynamics of an electron transfer reaction will impact the rate constant, and consequently we should expect that presence of dispersion in one parameter will then imply dispersion in the other parameter. The separation is only a valid approximation

when one of the dispersed parameters can be assumed to be a point value with reasonable accuracy, as is the case with low values of the $E^0\sigma$ parameter, or a distribution of $k_0$ values which are largely reversible.

Our proposal for using these results to distinguish different forms of dispersion is to compare experimental data against non-dispersed simulations, and select which dispersion parameter it is necessary to include in the model based on the observed discrepancy. Furthermore, it is our experience that the best medium for this comparison is the ramped harmonics. If it is possible to obtain a good fit between the lower-order ramped harmonics, but the simulated magnitude for the higher harmonics is too large, and the experimental harmonics are broader than predicted by the simulation, then it is likely that $E^0$ dispersion is present. If it is the case that the discrepancy is only in the magnitude, then the dispersion is likely kinetic, as long as the experimentalist is confident that the uncompensated resistance is not causing this effect. This method requires non-dispersed simulations that are a reasonably good fit to existing experimental data. These simulations could be generated using our existing workflows for automatic fitting processes, as briefly described in the introduction and laid out in more detail in previous work.[2] The inspiration for this paper came from this automated fitting process; when fitting PSV data,[23] we found that we could fit PSV data without dispersion, but when comparing the resultant ramped-FTACV simulation to the data, we discovered a discrepancy between experimental data and simulation that could only be explained by the presence of thermodynamic dispersion. Because the simulation of a non-dispersed current is $N_b^{n_p}$ times faster than simulating dispersed current (i.e. the number of bins or nodes to the power of the number of dispersed parameters), the time impact of the additional non-dispersed fitting attempts is relatively light. These non-dispersed simulations could be generated heuristically, but this comes with all the attendant issues with heuristic fitting, as discussed in.[14]
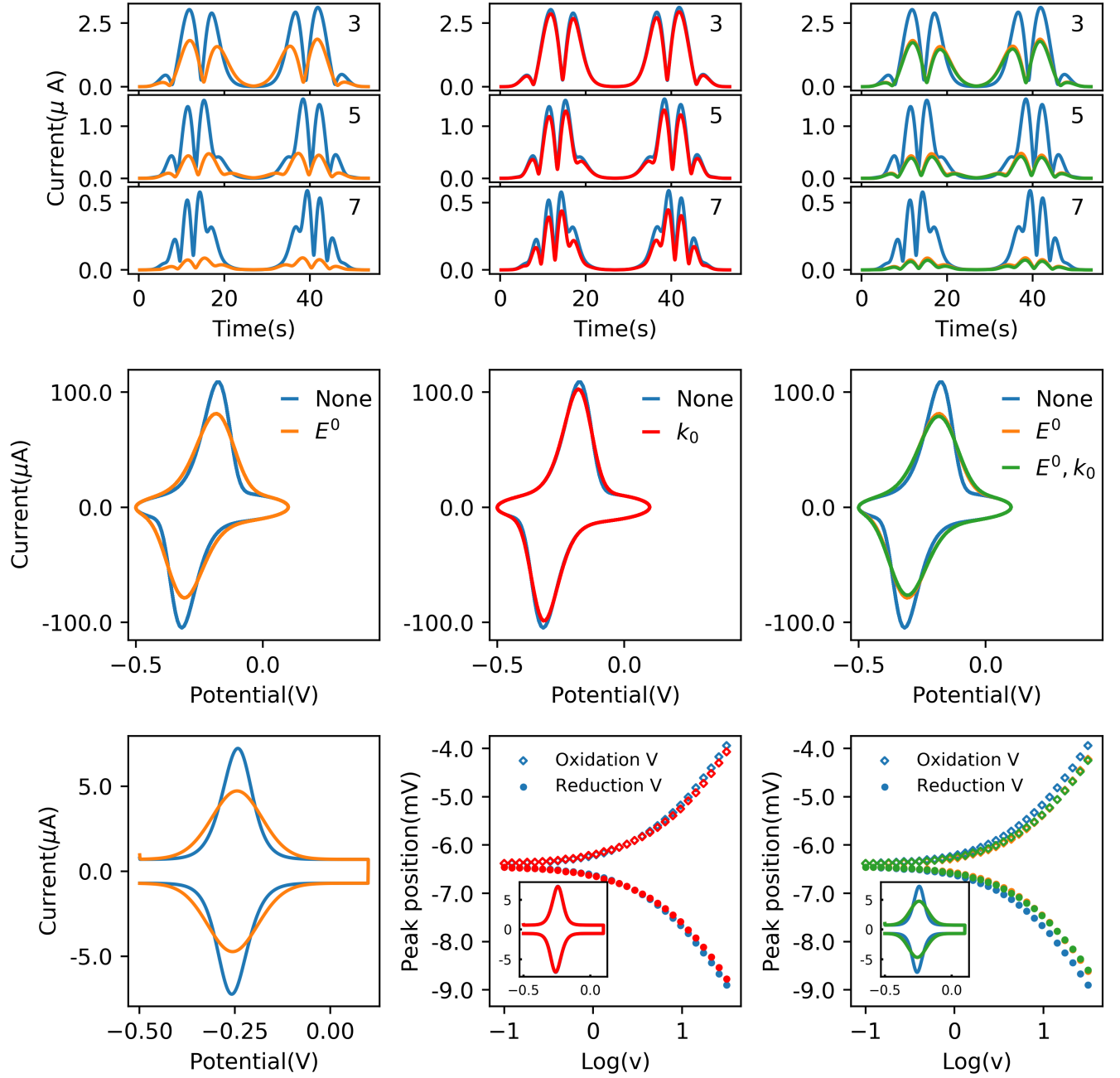
Figure 5: Comparison of different forms of dispersion for ramped FTACV, PSV and DCV. Each column represents a different form of dispersion, compared against the non-dispersed case (labelled as "None"). From left to right, the dispersed parameters are $E^0$, $k_0$ and a combination of the two, as listed in the legend of the middle row. All parameters are as in table 1.

# Supporting Information Available

Figures 2-4 are repeated with lower values of the kinetic parameter. Figures 5 is repeated with the kinetic parameter in both totally reversible and irreversibly regimes. We also include a figure on maximising the discrepancy between dispersed and non-dispersed systems by changing the frequency

# Acknowledgement

# References

(1) Adamson, H.; Robinson, M.; Bond, P. S.; Soboh, B.; Gillow, K.; Simonov, A. N.; Elton, D. M.; Bond, A. M.; Sawers, R. G.; Gavaghan, D. J., et al. Analysis of HypD disulfide redox chemistry via optimization of fourier transformed ac voltammetric data. *Analytical chemistry* **2017**, *89*, 1565–1573.

(2) Gavaghan, D. J.; Cooper, J.; Daly, A. C.; Gill, C.; Gillow, K.; Robinson, M.; Simonov, A. N.; Zhang, J.; Bond, A. M. Use of Bayesian inference for parameter recovery in DC and AC Voltammetry. *ChemElectroChem* **2018**, *5*, 917–935.

(3) Bieniasz, L.; Speiser, B. Use of sensitivity analysis methods in the modelling of electro-

chemical transients: Part 3. Statistical error/uncertainty propagation in simulation and in nonlinear least-squares parameter estimation. *Journal of Electroanalytical Chemistry* **1998**, *458*, 209–229.

(4) Zouraris, D.; Karantonis, A. Determination of kinetic and thermodynamic parameters from large amplitude Fourier transform ac voltammetry of immobilized electroactive species. *Journal of Electroanalytical Chemistry* **2020**, *876*, 114729.

(5) Bell, C. G.; Anastassiou, C. A.; O'Hare, D.; Parker, K. H.; Siggers, J. H. Theory of high frequency, large-amplitude sinusoidal voltammetry for ideal surface-confined redox systems. *Electrochimica acta* **2011**, *56*, 7569–7579.

(6) Laviron, E. General expression of the linear potential sweep voltammogram in the case of diffusionless electrochemical systems. *Journal of Electroanalytical Chemistry and Interfacial Electrochemistry* **1979**, *101*, 19–28.

(7) Robinson, M.; Ounnunkad, K.; Zhang, J.; Gavaghan, D.; Bond, A. Integration of Heuristic and Automated Parametrization of Three Unresolved Two-Electron Surface-Confined Polyoxometalate Reduction Processes by AC Voltammetry. *ChemElectroChem* **2018**, *5*, 3771–3785.

(8) Rowe, G. K.; Carter, M. T.; Richardson, J. N.; Murray, R. W. Consequences of kinetic dispersion on the electrochemistry of an adsorbed redox-active monolayer. *Langmuir* **1995**, *11*, 1797–1806.

(9) Clark, R. A.; Bowden, E. F. Voltammetric peak broadening for cytochrome c/alkanethiolate monolayer structures: dispersion of formal potentials. *Langmuir* **1997**, *13*, 559–565.

(10) Zhang, Z.; Rusling, J. F. Electron transfer between myoglobin and electrodes in thin films of phosphatidylcholines and dihexadecylphosphate. *Biophysical chemistry* **1997**, *63*, 133–146.

(11) Morris, G. P.; Baker, R. E.; Gillow, K.; Davis, J. J.; Gavaghan, D. J.; Bond, A. M. Theoretical analysis of the relative significance of thermodynamic and kinetic dispersion in the dc and ac voltammetry of surface-confined molecules. *Langmuir* **2015**, *31*, 4996–5004.

(12) Salverda, J. M.; Patil, A. V.; Mizzon, G.; Kuznetsova, S.; Zauner, G.; Akkilic, N.; Canters, G. W.; Davis, J. J.; Heering, H. A.; Aartsma, T. J. Fluorescent cyclic voltammetry of immobilized azurin: direct observation of thermodynamic and kinetic heterogeneity. *Angewandte Chemie International Edition* **2010**, *49*, 5776–5779.

(13) Patil, A. V.; Davis, J. J. Visualizing and tuning thermodynamic dispersion in metalloprotein monolayers. *Journal of the American Chemical Society* **2010**, *132*, 16938–16944.

(14) Bond, A. M. A perceived paucity of quantitative studies in the modern era of voltammetry: prospects for parameterisation of complex reactions in Bayesian and machine learning frameworks.

(15) Léger, C.; Jones, A. K.; Albracht, S. P.; Armstrong, F. A. Effect of a dispersion of interfacial electron transfer rates on steady state catalytic electron transport in [NiFe]-hydrogenase and other enzymes. *The Journal of Physical Chemistry B* **2002**, *106*, 13058–13063.

(16) Hexter, S. V.; Grey, F.; Happe, T.; Climent, V.; Armstrong, F. A. Electrocatalytic mechanism of reversible hydrogen cycling by enzymes and distinctions between the major classes of hydrogenases. *Proceedings of the National Academy of Sciences* **2012**, *109*, 11516–11521.

(17) Gessner, P. K.; Hasan, M. M. Freundlich and Langmuir isotherms as models for the adsorption of toxicants on activated charcoal. *Journal of pharmaceutical sciences* **1987**, *76*, 319–327.

(18) Stevenson, G. P.; Baker, R. E.; Kennedy, G. F.; Bond, A. M.; Gavaghan, D. J.; Gillow, K. Access to enhanced differences in Marcus–Hush and Butler–Volmer electron transfer theories by systematic analysis of higher order AC harmonics. *Physical Chemistry Chemical Physics* **2013**, *15*, 2210–2221.

(19) Adamson, H.; Bond, A. M.; Parkin, A. Probing biological redox chemistry with large amplitude Fourier transformed ac voltammetry. *Chemical Communications* **2017**, *53*, 9519–9533.

(20) Laborda, E.; Henstridge, M. C.; Batchelor-McAuley, C.; Compton, R. G. Asymmetric Marcus–Hush theory for voltammetry. *Chemical Society Reviews* **2013**, *42*, 4894–4905.

(21) Viswanathan, V.; Hansen, H. A.; Rossmeisl, J.; Jaramillo, T. F.; Pitsch, H.; Nørskov, J. K. Simulating linear sweep voltammetry from first-principles: application to electrochemical oxidation of water on Pt (111) and Pt3Ni (111). *The Journal of Physical Chemistry C* **2012**, *116*, 4698–4704.

(22) Bond, A. M.; Duffy, N. W.; Guo, S.-X.; Zhang, J.; Elton, D. Changing the look of voltammetry. 2005.

(23) Lloyd-Laney, H.; Yates, N.; Robinson, M.; Hewson, A. R.; Firth, J.; Zhang, J.; Elton, D.; Bond, A.; Parkin, A.; Gavaghan, D. Using Purely Sinusoidal Voltammetry for Rapid Parameterization of Surface-Confined Electrochemistry. **2020**,